THE JOURNAL OF PHYSICAL CHEMISTRY B

Article

pubs.acs.org/JPCB

Investigation of Structure and Crystallization Behavior of Poly(butylene succinate) by Fourier Transform Infrared Spectroscopy

Shu-Fang Yao, Xiao-Tong Chen, and Hai-Mu Ye*

Department of Materials Science and Engineering, China University of Petroleum, 102249 Beijing, P. R. China

Supporting Information

ABSTRACT: The detailed structure and crystallization behavior of poly(butylene succinate) (PBS) have been investigated by Fourier transform infrared (FTIR) and other methods systematically. For the first time, we confirmed that the C═O stretching modes of PBS can respond to three distinguish absorption bands in the FTIR spectrum, at around 1736, 1720, and 1714 cm^{-1} respectively. The 1736 cm^{-1} band is adopted as the stretching mode of C═O groups in free amorphous fraction (MAF); the 1714 cm^{-1} band which is relevant to more stable structure, displays more anisotropic in polarized FTIR spectra, and has been confirmed as stretching vibrations of hydrogen-bonded C═O groups in the crystalline phase. The 1720 cm^{-1} band is linked to crystallization but comes from less ordered structure. Moreover, the 1720 cm^{-1} band can be destroyed prior to 1714 cm^{-1} band during heating and constructed behind 1714 cm^{-1} band during cooling. Thus, the 1720 cm^{-1} band is reasonably ascribed to the C═O groups in rigid amorphous fraction (RAF) or intermediate phase which locates between MAF and crystalline phase. The corresponding investigation by differential scanning calorimetry (DSC) and wide-angle X-ray diffraction (WAXD) further supports that the three particular C═O absorption bands indeed reveal the typical three-phase structure for PBS. More important, the FTIR spectrum of PBS is very sensitive to sample preparation process and measurement mode. The relative content of each band depends on the crystallization temperature (T_c) and measured thickness. The higher T_c, the more RAF content appears when measured at room temperature; the thinner penetration thickness of FTIR measurement, the less RAF content can be detected, and the penetration thickness-dependent behavior is suggested as the result of higher mobility of chains in the air/bulk surface. Additionally, the particular three absorption bands of C═O groups in PBS force us to carefully reconsider previous reports on structure and interaction state obtained by FTIR spectroscopy in PBS and its composites.

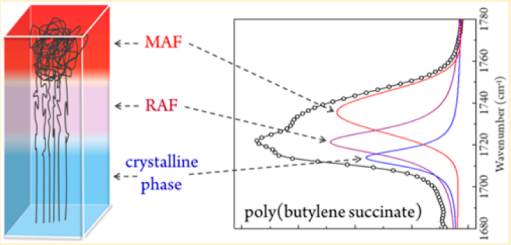

INTRODUCTION

Since there is incompletely decoupling between the fractions of random coils in the amorphous phase and the crystals in semicrystalline polymers, a three-phase model including mobile amorphous fraction (MAF), rigid amorphous fraction (RAF), and crystalline phase is considered to be superior to a two-phase model which only consists of MAF and crystalline phase.[1] When the coupling effect is strong enough, RAF is produced more and becomes significant, in which the chain segments involved are impacted by the interfacial geometrical constraints imposed by the neighboring crystalline phase and cannot move as free as them in MAF.[2] It is also suggested that RAF consisting of different molecular segments with somewhat different chain conformation, i.e., the intermediate phase region, can appear some similar but different properties from that of the MAF and crystalline phase. Up to now, it has been demonstrated that RAF exists in almost all types of semicrystalline polymer, such as polyethylene (PE), polypropylene (PP), polyamide (PA), poly(ethylene terephthalate) (PET), polycarbonate (PC), poly(ether ether ketone) (PEEK), poly(phenylenesulfide) (PPS), polyhydroxyalkanoate (PHA).[1,3−10] Furthermore, the existence of RAF is proved to be associated with appearance of lamellar stacks.[9−11] The dimensions of such intriguing interface could be estimated to be about 2−4 nm in poly(*R*-3-hydroxybutyrate-*co*-*R*-3-hydroxyvalerate) (PHBV) and PE.[10,12,13] The thinnest one has been reported in low molecular weight linear PE.[3] And some new improtant findings had been reported when RAF was considered to exist in semicrystalline polymers. Xu and Cebe applied the three-phase model to interpret the structure of cold-crystallized isotactic polystyrene (*i*-PS); they found that the RAF developed parallel to the development of crystalline phase and a specific annealing peak (T_a) was caused by irreversible relaxation of the RAF.[14] Pak et al. reported that the disappearance of RAF went together with melting crystals for poly(oxy-2,6-dimethyl-1,4-phenylene).[15] Di et al. comfirmed that RAF was a conclusive part in the crystallize process of PHB, where the crystallization could only complete when the RAF was sufficiently mobilized with increasing temperature, resulting in chain rearrangements.[16]

Poly(butylene succinate) (PBS), a biodegradable polyester with good mechanical performances, has received extensive study in last decades.[17] The thermal history of PBS determines its final structures of crystalline and amorphous phases, and the three-phase structure has been proposed for describing the

Received: August 10, 2017
Revised: September 20, 2017
Published: September 21, 2017

DOI: 10.1021/acs.jpcb.7b07954
J. Phys. Chem. B 2017, 121, 9476−9485

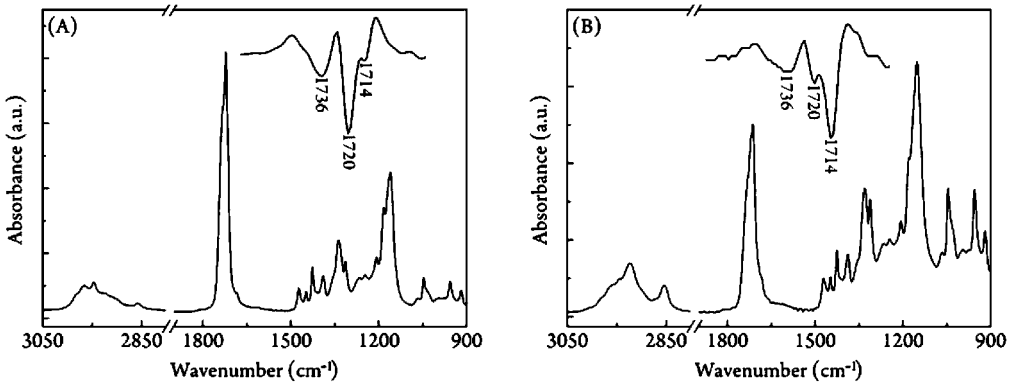

Figure 1. FTIR spectra of PBS measured by TR mode (A) and ATR mode (B).

aggregate structure of semicrystalline PBS.[18−22] Li group systematically studied the multiple melting behavior of melt-crystallized PBS samples and explained the annealing peak (T_a) as a result of the relaxation of RAF, since T_a only appeared in the nonreversible heat flow curve in the modulated DSC scan and its peak temperature and magnitude increased evidently with increasing annealing temperatures and time spans.[19] Signori et al. revealed the content of RAF in PBS could reach as high as 30% in PBS/hemp nanocomposites.[22]

Similar to other polymers, PBS, however, suffers some drawbacks, including brittle and easily aging problems.[23] To overcome these problems and broaden the versatility of PBS, considerable researches have been carried out using physical blending and copolymerization methods.[24−31] And the Fourier transform infrared (FTIR) spectroscopy has been frequently employed to verify the modification effect and explore the modification mechanism, especially studying FTIR absorption bands of carbonyl (C═O) groups.[32−48] For example, Qi et al. assigned the 1715 cm^{-1} band to C═O groups in crystalline region of neat PBS and attributed the 1722 cm^{-1} band to C═O groups of PBS hydrogen-bonding with the hydroxyl (−OH) groups on attapulgite surface in PBS/attapulgite composites.[40] In contrast, Luo et al. attributed the 1713 cm^{-1} band in PBS/bisphenol blends to the C═O groups hydrogen-bonding with −OH groups of bisphenol.[32] When we tried to summarize the law of FTIR absorption bands for C═O groups in PBS, some puzzling results, however, emerged. Although the absorption band around 1736 cm^{-1} has been consistently assigned to C═O groups in amorphous PBS, the corresponding band position for crystalline phase has been proposed in a wide range from 1728 to 1709 cm^{-1} in different studies.[41−43] Such large difference should not and cannot be simply recognized from instrument error or sample difference. Thus, it is vitally important to make the mechanism of C═O stretching vibrations clear before we can use FTIR to study PBS structure correctly. After trying our best to review all FTIR spectra of PBS-related, we found that the absorption bands assigned to the crystalline C═O groups of PBS were apt to locate around low wavenumber position (~1714 cm^{-1}) when nanomaterials like silica, isocyanate-modified fumed silica and organo-montmorillonite were introduced.[43−45] But, once the experiment is performed in high temperature range, the crystalline C═O band at high wavenumber position (~1720 cm^{-1}) tends to appear dominantly.[33,40] Adding nanomaterials usually benefits the decreasing of spherulite size, while raising experimental temperature prefers formation of larger spherulite. Thus, it is wondered whether the crystalline C═O band position related to the spherulite size? Of course, spherulite size should not be the intrinsic reason. Therefore, further studies are definitely needed to carry out.

If the three-phase model and the three observed FTIR absorption regions of C═O groups were combined, it is questioned whether the FTIR signals could rightly reflect the three-phase structure of semicrystalline PBS. Referentially, Khasanah et al. revealed that 1750, 1731, and 1722 cm^{-1} absorption bands of ultrathin PHB film respectively stem from the MAF, intermediate phase, and highly ordered crystalline state.[48] Therefore, in this study, FTIR spectroscopy, together with other characterizations, is used to systematically study the C═O stretching mode of PBS. The results demonstrate for first time that neat PBS can show three distinct FTIR absorption bands of C═O groups at 1736, 1720, and 1714 cm^{-1} which are further proven to respectively originate from the MAF, RAF (or intermediate phase) and crystalline phase, and sample thickness is a key factor that effects the C═O stretching absorption behavior. This study provides a fundamental for FTIR study on the structure and interaction state in PBS and its composites.

EXPERIMENTAL SECTION

Materials. PBS is synthesized from 1,4-butanediol and succinic acid by a two-step reaction of esterification and polycondensation in molten state, as reported in previous literature.[47] The polymerization product was first dissolved in chloroform ($CHCl_3$, AR grade) at a concentration of 5% (w/v), then the solution was centrifuged at a rate of 1000 rpm for 20 min. Consequently, the clear liquid was separated and precipitated in an excess amount of methanol (AR grade) at room temperature. After that, the precipitate was filtered and dried in a vacuum at 60 °C for 24 h. The number-average molecular weight (M_n) and polydisperse index (PDI) were measured by GPC as 7.74×10^4 g/mol and 1.48, respectively.

FTIR Measurement. PBS film for FTIR measurement was prepared by pouring 10 μL 2 wt % its solution of chloroform on a round CaF_2 window with pipet, except for the room-temperature oriented sample with a drawn ratio of 300%. Experiments were carried out on a Bruker Tension II/Hyperion FTIR spectrometer by averaging signal over 32 scans in the wavenumber range of 4000−800 cm^{-1}. Temperature-dependent FTIR was carried out using THMS-600 hot-stage accessory (Linkam Scientific Instrument Ltd.). Both transmission (TR) mode and attenuated total reflectance (ATR) mode FTIR were employed.

DOI: 10.1021/acs.jpcb.7b07954
J. Phys. Chem. B 2017, 121, 9476−9485

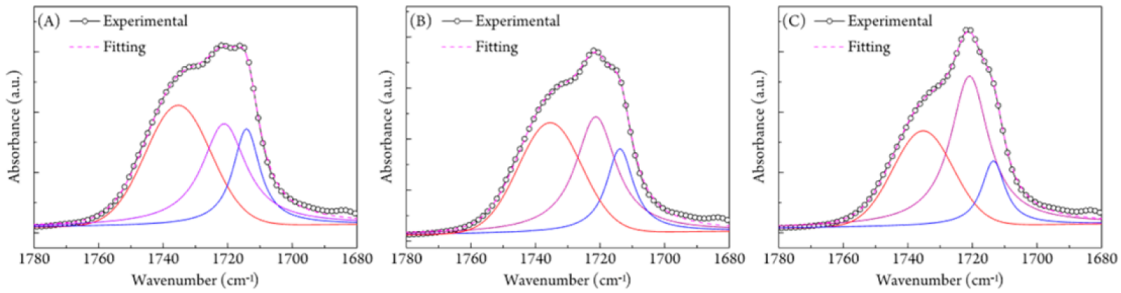

Figure 2. FTIR spectra (from 1780 to 1680 cm^{-1}) of a PBS melt-crystallized completely at different T_cs: 60 °C (A), 80 °C (B), and 95 °C (C).

The film was first heated to 150 °C and held for 3 min to eliminate any thermal history, following by quickly transferring to a hot-stage with prefixed temperature (60−95 °C) to crystallize completely or by a nonisothermally crystallization process, then the film was used to collect its FTIR spectrum at room temperature. The *in situ* collection of heating and cooling FTIR spectra was manipulated by recording every 30 s interval in a heating/cooling rate of 10 °C/min measurements. To obtain the polarized FTIR for oriented samples, a ZnSe IR polarizer accessory was employed. The thicknesses of film were measured by micrometer or SEM method.

WAXD Measurement. Wide angle X-ray diffraction (WAXD) analysis was performed on a Bruker AXS D8 Advance powder diffractometer using Cu Kα radiation (λ_{Cu} = 0.15405 nm) under 25 °C. The diffractograms were collected in the 2θ range interval from 10° to 30° at a scanning rate of 2°/min.

DSC Measurement. The crystallization and melting behavior of samples was investigated by a differential scanning calorimeter (DSC, NETZSCH-204F1) equipped with an intercooler as the cooling system under argon atmosphere. The samples were weighed at around 5.0 mg and sealed in aluminum pans.

Polarized Optical Microscope. The spherulitic morphology and crystallization process of samples were captured on a Leica DM2500P polarized optical microscope (POM) instrument equipped with a Linkam THMS600 hot-stage.

RESULTS AND DISCUSSION

FTIR absorption of C═O Groups of PBS. Figure 1 illustrates the FTIR spectra of PBS obtained by TR and ATR modes. The sample was prepared by nonisothermally crystallizing PBS melt from 150 °C at a rate of 10 °C/min. It is evident that there are three absorption bands of C═O stretching modes at 1736, 1720, and 1714 cm^{-1} in Figure 1, parts A and B, which are much clearer in the inserted second derivative spectra. To validate the universality that there are three C═O stretching modes for neat semicrystalline PBS, two other sourced PBS samples, an industrial and a lower molecular weight, were also employed to collect their FTIR spectra. It was found that they could also exhibit three absorption bands of C═O stretching modes (Figure S1 in the Supporting Information). Thus, neat semicrystalline PBS can display three distinct C═O absorption bands, which is raised and affirmed for the first time here. The difference in spectra between TR and ATR modes might be due to their differences in incident optical geometry, penetration thickness and some other reasons, which will be further analyzed in the Discussion.

As summarized in the Introduction, the C═O absorption bands have been captured for PBS under various situations. The 1736 cm^{-1} band has been consistently assigned to the stretching mode of C═O groups in free amorphous region, while the assignments of 1720 and 1714 cm^{-1}, especially for 1720 cm^{-1}, for neat PBS are still quite promiscuous.[32−40] Considering the dependence of C═O absorption bands of PBS on situation, a PBS film with 7 μm in thickness was prepared and melt-crystallized at different crystallization temperatures (T_cs) from 60 to 95 °C, and the corresponding FTIR spectra between 1780 and 1680 cm^{-1} measured at room temperature are present in Figure 2 and Figure S2. All spectra show three C═O absorption bands but with different relative intensities. A deconvolution method was used to obtained relative contents of bands at 1736, 1720, and 1714 cm^{-1}, and their values are plotted as line charts in Figure 3. The relative content of 1736

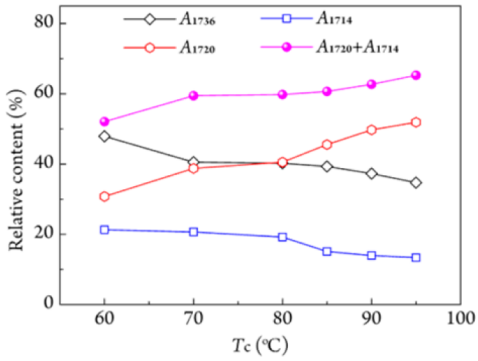

Figure 3. Relative contents of different C═O absorption bands at different T_cs.

cm^{-1} band arisen from C═O in free amorphous phase decreases slightly with increasing T_c, so does the relative content of 1714 cm^{-1} band. However, the relative content of 1720 cm^{-1} band increases slightly and steadily with increasing T_c. This changing tendency is similar to the previous observation that PBS crystallized at high T_c shows a C═O absorption band around 1720 cm^{-1}.[33,40] PBS samples melt-crystallized in the T_c range all adopt the same α-form crystal modification (Figure 4). On the basis of the red-shift behavior and semicrystalline structure, the 1720 and 1714 cm^{-1} bands are believed to relate to the formation of crystalline structure. The crystal lattices should have the strongest confinement effect (including physical and hydrogen-bonding) on C═O groups in the lamellar structure of PBS crystal, so the 1714 cm^{-1} band is more reasonable than 1720 cm^{-1} to be assigned to the C═O in crystal lattices. More important, due to the fact that crystal lattice structure of PBS is unchanged when changing T_c, the intensity ratio between 1720 and 1714 cm^{-1} would have been fixed, should the 1720 cm^{-1} be from, *i.e.*, unhydrogen-bonded C═O groups in the lattices too. There-

DOI: 10.1021/acs.jpcb.7b07954
J. Phys. Chem. B 2017, 121, 9476−9485

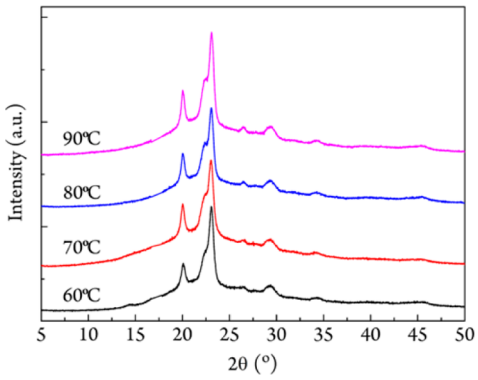

Figure 4. Wide-angle X-ray diffractograms of PBS crystallized completely at different temperatures.

fore, the 1720 cm^{-1} band of neat PBS is probably stemming from the RAF region or intermediate phase, which is in accordance with the state that the packing behavior of chain segments in RAF or intermediate phase is less ordered and looser than in the crystalline phase, but more highly ordered and denser than in MAF. To get a brief description, the intermediate phase will be also termed as RAF in the following.

The slightly increasing content of 1720 cm^{-1} with increasing T_c indicates that RAF rises somewhat with increasing T_c. This phenomenon is in according with Li group's research conclusion on the annealing peak (T_a) of PBS. They demonstrated that T_a is related to the RAF of PBS and the magnitude (enthalpy-involved relaxation) of T_a increased as the consequence of raising T_c.[19] The apparent relative content of 1720 cm^{-1} band calculated by FTIR data, 33% to 52% for T_c ranging between 60 and 95 °C, might be possibly seemed too high to be expected for RAF content in semicrystalline polymers. Nevertheless, some research groups had reported that the RAF content for PBS and its composites could reach as high as 14−37% by DSC and dielectric spectroscopy.[22,49,50] Of course, due to the different infrared absorption coefficients of C═O groups in among crystalline phase, RAF and MAF, the relative contents of such three structural parts of semicrystalline PBS could not be the real contents. Amorphous phase is seemed to possess larger absorption coefficient than crystalline phase. So, some deviations must exist from the real contents but the changing tendency, however, should be the same for relative contents obtained by FTIR and real contents.

Polarized FTIR. Figure 5 shows the polarized FTIR spectra of oriented semicrystalline PBS film which had been stretched

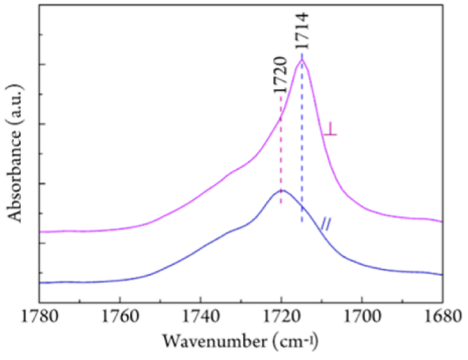

Figure 5. Polarized FTIR spectra of the oriented PBS film within the wavenumber range of 1780−1680 cm^{-1}.

to an elongation of 300% under room temperature. It is of interest to find that 1714 cm^{-1} band is much more significant in the perpendicularly polarized FTIR spectrum where the chain direction in crystal region is perpendicular to incident polarized infrared. Since the C═O direction in PBS lattice is perpendicular to the chain direction, the 1714 cm^{-1} band is now further confirmed to corresponding the C═O stretching mode in crystalline phase. In a recent study, we only observed a C═O absorption band at 1716 cm^{-1} for extended-chain crystals of PBS whose crystallinity is higher than 94%.[51] However, the 1720 cm^{-1} band can be observed with similar absorption intensity in perpendicularly and parallelly polarized FTIR spectra, indicating the relevant structure is less oriented, or even close to random orientating state. Therefore, C═O groups related to 1720 cm^{-1} must be located outside the crystalline phase and should be assigned to the RAF.

Temperature-Dependent FTIR. Figure 6 illustrates the collecting FTIR spectra and differential spectra of PBS during the heating process from 50 to 120 °C. Obviously, the intensity of 1736 cm^{-1} band increases and those of 1720 and 1714 cm^{-1} bands decrease gradually during heating, corresponding to the fact that the two bands at lower wavenumber position are connected with crystalline structure. To get a detailed relationship between 1720 and 1714 cm^{-1}, 2D-IR correlation analysis, by which overlapping bands can be clearly reflected,[52,53] was employed. Figure 7 shows the computed synchronous and asynchronous 2D correlation spectra in the wavenumber range of 1730−1705 cm^{-1}, which are generated from the temperature-dependent FTIR spectra. Two autopeaks at (1720, 1720) cm^{-1} and (1714, 1714) cm^{-1} together with a pair of positive cross peaks at (1720, 1714) cm^{-1} appear in the synchronous 2D correlation spectrum. The peaks located at within the positive correlation spectral region indicate there is connection between 1720 and 1714 cm^{-1} bands besides the same decreasing tendency with raising temperature. In the corresponding asynchronous 2D correlation spectrum, a pair of cross peaks at (1720, 1714) cm^{-1} appear. The negative signal in $[\upsilon_1 > \upsilon_2]$ sector reveals that the disturbing factor, *i.e.*, heating, destroys the 1720 cm^{-1} band relevant structure prior to the 1714 cm^{-1} band relevant structure, demonstrating the 1720 cm^{-1} band relevant structure is less stable/ordered than the 1714 cm^{-1} band relevant structure. The synchronous 2D correlation spectra between C═O stretching modes and C−H stretching modes (Figure S3) were also calculated and presented in Figure S4. It can be observed that many cross peaks related to 1714 cm^{-1} band appear, including negative (2957, 1714) cm^{-1} and (2874, 1714) cm^{-1}, and positive (2946, 1714) cm^{-1} and (2857, 1714) cm^{-1}. Such phenomena present the destruct of hydrogen bonding interaction of C═O···C−H in crystalline phase.[54] Thus, 1714 cm^{-1} is from to the hydrogen-bonded C═O groups in crystalline phase. However, there is no cross peak related to 1720 cm^{-1} band, that is, the 1720 cm^{-1} band is not relative to hydrogen bonds.

Figure 8 collects the temperature-dependent FTIR spectra during melt-cooling process. The intensities of 1720 and 1714 cm^{-1} bands rise as that of amorphous fraction at 1736 cm^{-1} band decreases, which is in accordance with the occurrence of crystallization. Figure 9 presents the 2D correlation spectra. In the synchronous 2D correlation spectrum, only a strong autopeak of (1714, 1714) cm^{-1} develops and very weak positive correlated signals for both (1720, 1720) cm^{-1} and (1720, 1714) cm^{-1} appears. However, in the asynchronous 2D correlation spectrum, a pair of peaks of (1720, 1714) cm^{-1} arise and the

DOI: 10.1021/acs.jpcb.7b07954
J. Phys. Chem. B 2017, 121, 9476−9485

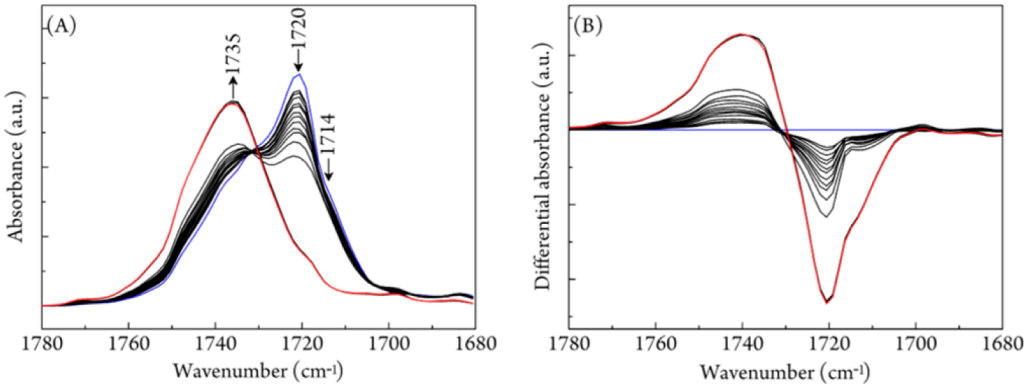

Figure 6. Temperature-dependent (A) and differential (B) FTIR spectra of PBS which was heated from 50 to 120 °C in the wavenumber range of 1780−1680 cm^{-1}. Arrows indicate the changing trends. The differential spectra were obtained by subtracting the initial spectra collected at 50 °C.

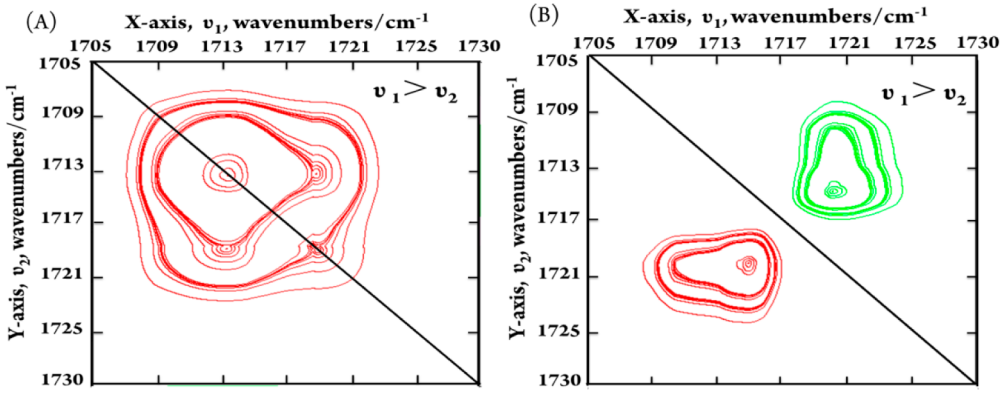

Figure 7. Synchronous (A) and asynchronous (B) 2D IR correlation spectra of neat PBS in the C═O stretching mode region generated from the temperature-dependent FTIR spectra in Figure 5A.

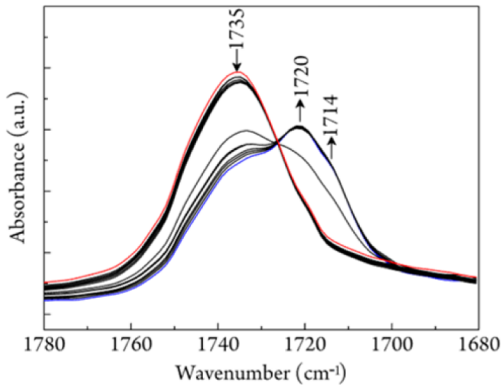

Figure 8. Temperature-dependent FTIR spectra of PBS which was cooled from 120 to 50 °C in the wavenumber range of 1780−1680 cm^{-1}. Arrows indicate the changing trends.

signal is positive in $[\upsilon_1 > \upsilon_2]$ sector, revealing the change of 1714 cm^{-1} band goes ahead of the change of 1720 cm^{-1}. The phenomenon is in conformity with many previous studies, where the RAF is proposed to form following, at nearly the same time, the formation of crystalline phase and exist by attaching to crystals.[1,9−11] The rather weak strength of (1720, 1720) cm^{-1} autopeak and (1720, 1714) cm^{-1} peak might be in accordance with the non-independence of RAF, although the 1720 cm^{-1} band displays more remarkable change than the 1714 cm^{-1} band.

Solvent Vapor Treatment. The vapor of good solvent for PBS can help enhance the chain mobility of RAF, and then possibly promotes the degree of crystallinity. Hence, $CHCl_3$ vapor was utilized to the semicrystalline PBS. Figure 10 shows the FTIR of semicrystalline PBS before and after treating in $CHCl_3$ vapor (1 mL $CHCl_3$ in 500 mL sealed beaker) for 15 h under room temperature. It was found that the relative content of 1714 cm^{-1} band increased from 11.4% to 18.2% and that of 1720 cm^{-1} fell from 44.6% to 38.9% with a slight increase of MAF content (1736 cm^{-1} band). The corresponding DSC tests in Figure S5 also show that the annealed peak (step) which relates to RAF is weakened.[19] Thus, the $CHCl_3$ vapor treatment experiment further ensures that 1714 and 1720 cm^{-1} bands originate, respectively, from C═O groups in the crystalline phase and RAF.

DISCUSSION

To obtain other quantitative description of RAF in PBS, DSC and WAXD were employed to analyze the three-phase structure of PBS. The DSC heating curves of PBS sample after completely crystallizing at different T_c were measured from −80 to 150 °C (Figure S6). The fractions of MAF were calculated by eq 1:

$$w_{MAF} = \frac{\Delta c_p}{\Delta c_p^s} \times 100\% \quad (1)$$

Here Δc_p is the specific heat capacity change of crystalline PBS during glass transition, Δc_p^s is the specific heat capacity of total amorphous PBS during glass transition and calculated as 0.52 J/

DOI: 10.1021/acs.jpcb.7b07954
J. Phys. Chem. B 2017, 121, 9476−9485

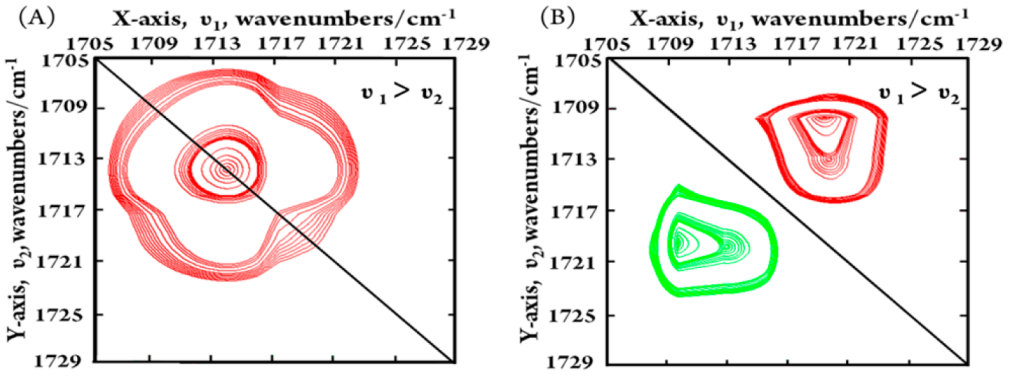

Figure 9. Synchronous (A) and asynchronous (B) 2D IR correlation spectra of neat PBS in the C═O stretching mode region generated from the temperature-dependent FTIR spectra in Figure 7.

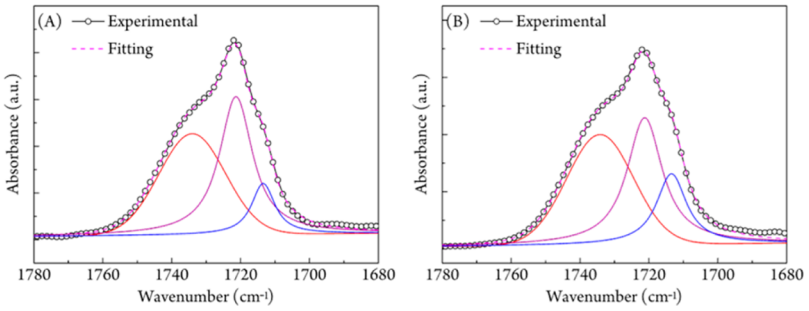

Figure 10. FTIR spectra of semicrystalline PBS before (A) and after (B) treating in $CHCl_3$ vapor for 15 h.

(g·K) from Figure S7. The fractions of crystalline phase were calculated by eq 2:

$$w_c = \frac{\Delta H_m}{\Delta H_m^0} \times 100\% \quad (2)$$

Here ΔH_m is the melting enthalpy of crystalline PBS during glass transition, and ΔH_m^0 is 110.3 J/g, which is calculated as the theoretical melting enthalpy of 100% crystalline PBS.[26,55] Then the fractions of RAF in crystalline PBS were worked out using eq 3:

$$w_{RAF} = 100\% - w_{MAF} - w_c \quad (3)$$

The T_c-dependent fractions of MAF, crystalline phase and RAF are shown in Figure 11. The content of MAF dips gradually with increasing T_c, so does the content of crystalline phase with a small degree. Though the values are different, the decreasing tendency measured using DSC agree with the changes of A_{1736} and A_{1714} in Figure 3. The content of RAF evidently rises with increasing T_c, which is responsible for the positive T_c-dependent change of 1720 cm^{-1} absorption band. However, values of relative contents of RAF from DSC are quite different from FTIR, and the reason might be ascribed to probable overestimation on crystallinity. Besides the effect of IR absorption coefficients and band overlapping, the value of ΔH_m^0 of PBS, 110.3 J/g, was taken on the basis of group contribution method,[55] and some complicated relaxation, melting and recrystallization behaviors always appear during the heating process of polymer.[14] When calculating the relative crystallinity w_c from WAXD data, it was found that the content of crystalline phase was quite lower than that measured by DSC and also showed a slightly negative T_c-dependent changing tendency (Figure 12). The consequent content of RAF

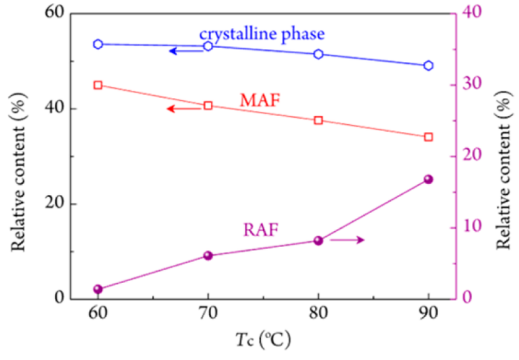

Figure 11. T_c-dependent trendencies of relative contents of MAF, RAF, and crystalline phase measured by DSC.

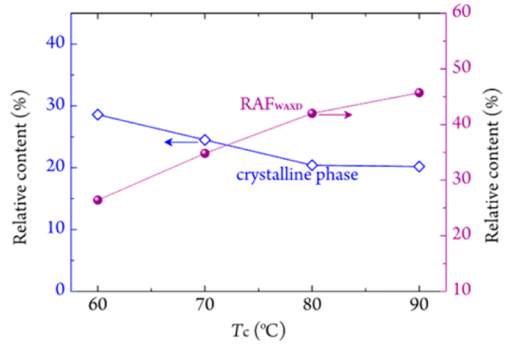

Figure 12. T_c-dependent trendencies of relative contents of RAF_{WAXD} and crystalline phase measured by WAXD.

DOI: 10.1021/acs.jpcb.7b07954
J. Phys. Chem. B 2017, 121, 9476−9485

(RAF_{WAXD}) increased with raising T_c. The similar changing tendency obtained by FTIR, DSC, and WAXD further confirms that 1736, 1720, and 1714 cm^{-1} bands are rightly assigned to MAF, RAF, and crystalline phase, respectively. Among the characterizing methods, FTIR can directly and markedly reveal the three-phase structure of PBS on the basis of the particular three C═O stretching modes.

What is the reason for the phenomenon that the higher preparation temperature for PBS sample the higher content of RAF occurs? First, we have to check what change had made when the PBS sample was transferred from T_c to room temperature. Figure 13 shows the spectra of PBS film after completely isothermal crystallization at 95 °C, then cooling to 25 °C and holding at 25 °C for 2 h, respectively. During the 95 to 25 °C process, the intensity of 1720 cm^{-1} strengthened with the weakening of 1736 cm^{-1} band; but the intensity of crystalline phase (1714 cm^{-1}) remained unchanged. Then, 2 h more treatment at 25 °C hardly led to any change. Therefore, when the sample was transferred from T_c to room temperature, some MAF devitrified to RAF due to the reduction of thermal drive from surrounding environment. Besides the C═O stretching modes, we could also find some other changes in FTIR spectra, including C−O stretching mode at 1340 cm^{-1} and CH_2 wagging mode at 1392 cm^{-1}. When the PBS film was isothermally crystallized completely at given T_c, higher T_c benefits the formation of perfect crystalline structure which would confine the mobility of nearby amorphous chain segments more strongly and results in more RAF content. Meanwhile, the content of RAF is promoted from MAF during the cooling process to room temperature. When flexible noncrystallizable comonomers, *e.g.*, butylene adipate units, were introduced into the chains, the RAF content declined.[49] The easy physical aging of PBS should be due to the high RAF content and copolymerization can be utilized to overcome such drawback by reducing RAF content.

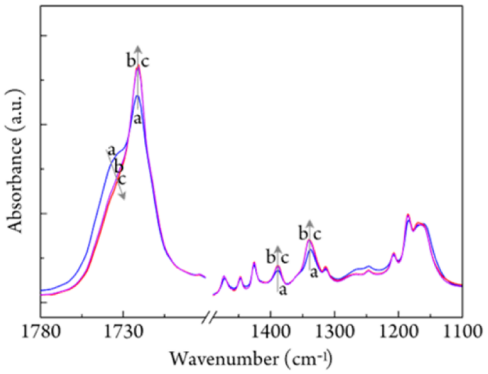

Figure 13. FTIR spectra of PBS film after completely isothermal crystallization at 95 °C (a), then cooling to 25 °C (b) and holding at 25 °C for 2 h (c).

As questioned in Figure 1, what is responsible for the difference in spectra between TR and ATR modes for the same sample need further study. The appearing 1720 cm^{-1} band in the TR spectrum is stronger than in the ATR one, in contrast, 1714 cm^{-1} band in the ATR spectrum is more remarkable than in the TR one. FTIR spectra of PBS and nucleated PBS in Figure S8 confirm that the spherulite size is not the cause of different C═O bands. The thickness of TR measured sample was about 7 μm, while the penetration depth of ATR mode was less than 2.01 μm (information from the instruction of FTIR instrument, ZnSe crystal). Thus, the surface effect which has been widely reported to induce significant properties between polymer chains in surface layer and inner bulk probably plays an important role in the IR absorption behavior. Figure 14 depicts the TR spectra of PBS film with thicknesses of 15, 1, and 0.2 μm. Interestingly, the relative content of 1720 cm^{-1} band decreased with increasing thickness of film, while contrast

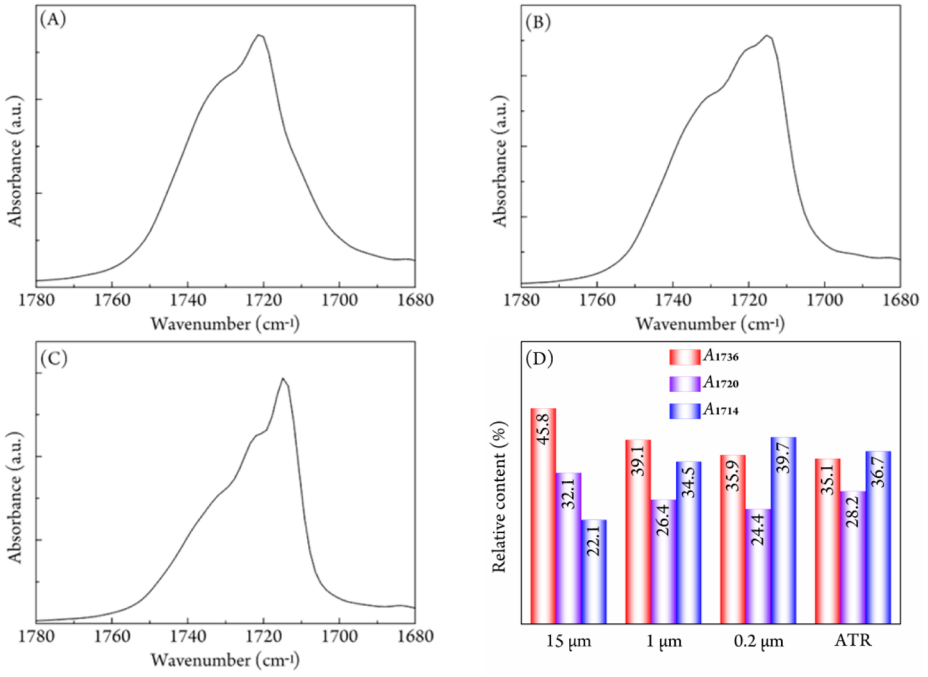

Figure 14. TR mode FTIR spectra of PBS films with different thicknesses, 15 μm (A), 1 μm (B), and 0.2 μm (C). The relative contents of three bands in four different sample are charted in part D. All the films were performed using the same melt-crystallization process.

DOI: 10.1021/acs.jpcb.7b07954
J. Phys. Chem. B 2017, 121, 9476−9485

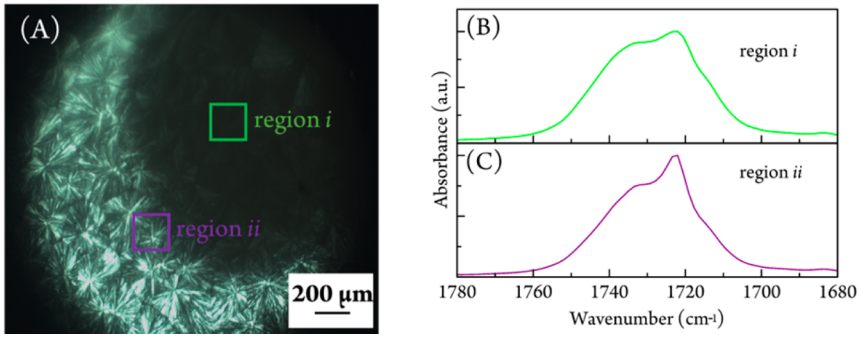

Figure 15. POM image of coffee ring structual PBS film(A) and the region-selected FTIR spectra of region *i* (B) and region *ii* (C).

tendency for the 1714 cm^{-1} band. The 1720 cm^{-1} band was the major band for C═O stretching modes when film thicknesses were 7 and 15 μm, but the 1714 cm^{-1} band changed, instead, into the major band for films with thicknesses of 1 μm and 20 nm. Besides, the spectrum of PBS film with thickness about 1 μm (Figure 14B) was quite similar to the ATR mode spectrum (Figure S9). Figure 14D charts the relative contents of C═O stretching bands in different PBS samples. The relative content of MAF decreases with decreasing film thickness, so does the relative content of RAF, but the relative of crystalline phase increases with decreasing film thickness. In particular, the relative contents for three parts measured by TR mode from PBS film about 1 μm are very close to those measured by ATR mode. Therefore, film thickness (or penetration depth) is believed to be a crucial factor determining the FTIR absorption behavior of C═O groups in PBS.

To eliminate any possible existing difference of thermal treatment among different films, a PBS film with coffee ring structure was prepared and region-selected FTIR measurements (200 × 200 μm^2) were carried out. Figure 15A shows the polarized image of PBS film. Low birefringence intensity indicates the corresponding "region *i*" is thinner than "region *ii*" with high birefringence intensity. It is evident in their corresponding FTIR spectra (Figure 15B and 15C) that the thicker the film, the more appearance of 1720 cm^{-1} band and the less appearance of 1714 cm^{-1} band. So, thickness of film affects the FTIR spectra of PBS significantly, that is, the film surface which is placed in the interface between bulk and air is an essential influencing component of C═O stretching modes. Many studies have supported that relaxation of polymer chains in the surface of bulk outpaces that in bulk.[56−59] For example, the chain relaxation of polystyrene has been found to occur almost 50% faster in the surface than in the bulk, and polymer chains in the air/polymer interface possessing higher mobility than in bulk is expected to be a universal property of polymeric chains.[58] Enhancing the mobility and accelerating the relaxation of polymer chains would go against the formation of RAF and benefit the formation of crystalline structure. Subsequently, the more surface content involved into the FTIR absorption, the less remarkable signal of RAF band, *i.e.*, 1720 cm^{-1} and the more obvious signal of crystalline band, *i. e.* 1714 cm^{-1}. Additionally, similar ATR and TR FTIR spectra for low molecular weight in Figure S1 should be due to its high chain mobility, so the effect of thickness turns to less significant.

Owing to the response of three-phase structure in FTIR spectroscopy and the high sensitive of surface-related (thickness-dependent) absorption behavior we should pay exceeding caution on using FTIR spectroscopy to identify the relative crystallinity and verify special interaction between PBS and other substances, especially using the band around 1720 cm^{-1}. For example, Inoue and co-workers put forward the hydrogen-bonding interaction between PBS and cyclodextrins based on the existence of 1721 cm^{-1} when the sample was heated over 140 °C which was higher than the melting point of PBS.[33] There is no RAF in the molten state, so the conclusion is reliable. However, when we use the band around 1720 cm^{-1} to prove the interaction forming between PBS and other substances below melting point,[27,37−39] more evidence are need to further confirm it, because we could not distinguish the origin of 1720 cm^{-1} band from either PBS/other substance interaction or RAF in semicrystalline state just using the FTIR result.

CONCLUSIONS

In this study, we have systematically studied the FTIR spectra of C═O groups in PBS and, for the first time, confirmed the existence of the particular three absorption bands behavior in semicrystalline PBS, 1736, 1720, and 1714 cm^{-1}, which are stemmed from C═O stretching modes in the MAF, RAF (or intermediate phase) and crystalline phase, respectively. On one hand, the relative contents of 1736 and 1714 cm^{-1} bands respectively originated from C═O groups in MAF and crystalline phase decreases slightly, the relative content of 1720 cm^{-1} band, however, increases steadily with increasing T_c. On the other hand, the relative contents of three bands are significantly affected by the thickness of thin film and the measurement mode of FTIR; the thinner of film thickness, the appearance of 1714 cm^{-1} band. The thickness-dependent FTIR could be due to the polymer chains with higher mobility and easier relaxation in the air/bulk surface, which is against the formation of RAF.

Since the neat crystalline PBS can display three distinguish FTIR absorption bands of C═O stretching modes, we should be much more deliberate and careful when applying the FTIR signals to analyze the structure and interaction state of PBS and its composites.

ASSOCIATED CONTENT

Supporting Information

The Supporting Information is available free of charge on the ACS Publications website at DOI: 10.1021/acs.jpcb.7b07954.

Additional FTIR spectra, POM images of PBS and nucleated PBS, DSC curves of PBS, and 2D-FTIR spectra of PBS during heating (PDF)

DOI: 10.1021/acs.jpcb.7b07954
J. Phys. Chem. B 2017, 121, 9476−9485

AUTHOR INFORMATION

Corresponding Author

*(H.-M.Y) E-mail: yehaimu@cup.edu.cn.

ORCID

Hai-Mu Ye: 0000-0001-7566-9559

Notes

The authors declare no competing financial interest.

ACKNOWLEDGMENTS

This work was supported by the National Natural Science Foundation of China (NSFC, Grant No. 21674128) and China University of Petroleum (Beijing). We are grateful to Prof. Jun Xu from Tsinghua University for fruitful discussion.

REFERENCES

(1) Wunderlich, B. Reversible crystallization and the rigid–amorphous phase in semicrystalline macromolecules. *Prog. Polym. Sci.* **2003**, *28*, 383–450.

(2) Schick, C.; Wurm, A.; Mohamed, A. Vitrification and devitrification of the rigid amorphous fraction of semicrystalline polymers revealed from frequency-dependent heat capacity. *Colloid Polym. Sci.* **2001**, *279*, 800–806.

(3) Mandelkern, L.; Alamo, R. G.; Kennedy, M. A. The interphase thickness of linear polyethylene. *Macromolecules* **1990**, *23*, 4721–4723.

(4) Zia, Q.; Mileva, D.; Androsch, R. Rigid amorphous fraction in isotactic polypropylene. *Macromolecules* **2008**, *41*, 8095–8102.

(5) Chen, H.; Cebe, P. Investigation of the rigid amorphous fraction in Nylon-6. *J. Therm. Anal. Calorim.* **2007**, *89*, 417–425.

(6) Di Lorenzo, M. L.; Righetti, M. C.; Cocca, M.; Wunderlich, B. Coupling between crystal melting and rigid amorphous fraction mobilization in poly(ethylene terephthalate). *Macromolecules* **2010**, *43*, 7689–7694.

(7) Chen, H.; Cebe, P. Vitrification and devitrification of rigid amorphous fraction of PET during quasi-isothermal cooling and heating. *Macromolecules* **2009**, *42*, 288–292.

(8) Lu, S. X.; Cebe, P. Effects of annealing on the disappearance and creation of constrained amorphous phase. *Polymer* **1996**, *37*, 4857–4863.

(9) Schick, C.; Wurm, A.; Mohammed, A. Formation and disappearance of the rigid amorphous fraction in semicrystalline polymers revealed from frequency dependent heat capacity. *Thermochim. Acta* **2003**, *396*, 119–132.

(10) Esposito, A.; Delpouve, N.; Causin, V.; Dhotel, A.; Delbreilh, L.; Dargent, E. From a three-phase model to a continuous description of molecular mobility in semicrystalline poly(hydroxybutyrate-co-hydroxyvalerate). *Macromolecules* **2016**, *49*, 4850–4861.

(11) Androsch, R.; Wunderlich, B. The link between rigid amorphous fraction and crystal perfection in cold-crystallized poly(ethylene terephthalate). *Polymer* **2005**, *46*, 12556–12566.

(12) Tognana, S.; Salgueiro, W. Influence of the rigid amorphous fraction and segregation during crystallization in PHB/DGEBA blends. *Polym. J.* **2015**, *47*, 789–795.

(13) Cantow, H. J.; Kunz, M.; Klotz, S.; Möller, M. The net distribution of elements in multiphase polymer materials via element-specific electron microscopy. *Makromol. Chem., Macromol. Symp.* **1989**, *26*, 191–196.

(14) Xu, H.; Cebe, P. Heat capacity study of isotactic polystyrene: dual reversible crystal melting and relaxation of rigid amorphous fraction. *Macromolecules* **2004**, *37*, 2797–2806.

(15) Pak, J.; Pyda, M.; Wunderlich, B. Rigid amorphous fractions and glass transitions in poly(oxy-2,6-dimethyl-1,4-phenylene). *Macromolecules* **2003**, *36*, 495–499.

(16) Di Lorenzo, M. L.; Gazzano, M.; Righetti, M. C. The role of the rigid amorphous fraction on cold crystallization of poly(3-hydroxybutyrate). *Macromolecules* **2012**, *45*, 5684–5691.

(17) Xu, J.; Guo, B. H. Poly(butylene succinate) and its copolymers: research, development and industrialization. *Biotechnol. J.* **2010**, *5*, 1149–1163.

(18) Yoo, E. S.; Im, S. S. Melting behavior of poly(butylene succinate) during heating scan by DSC. *J. Polym. Sci., Part B: Polym. Phys.* **1999**, *37*, 1357–1366.

(19) Wang, X.; Zhou, J.; Li, L. Multiple melting behavior of poly (butylene succinate). *Eur. Polym. J.* **2007**, *43*, 3163–3170.

(20) Tai, H. J. Dielectric spectroscopy of poly (butylene succinate) films. *Polymer* **2007**, *48*, 4558–4566.

(21) Arandia, I.; Mugica, A.; Zubitur, M.; Mincheva, R.; Dubois, P.; Müller, A. J.; Alegría, A. The complex amorphous phase in poly(butylene succinate-ran-butylene azelate) isodimorphic copolyesters. *Macromolecules* **2017**, *50*, 1569–1578.

(22) Signori, F.; Pelagaggi, M.; Bronco, S.; Righetti, M. C. Amorphous/crystal and polymer/filler interphases in biocomposites from poly(butylene succinate). *Thermochim. Acta* **2012**, *543*, 74–81.

(23) Yasuniwa, M.; Satou, T. Multiple melting behavior of poly(butylene succinate). I. Thermal analysis of melt-crystallized samples. *J. Polym. Sci., Part B: Polym. Phys.* **2002**, *40*, 2411–2420.

(24) Qiu, Z.; Ikehara, T.; Nishi, T. Poly(hydroxybutyrate)/poly(butylene succinate) blends: miscibility and nonisothermal crystallization. *Polymer* **2003**, *44*, 2503–2508.

(25) Lai, S. M.; Huang, C. K.; Shen, H. F. Preparation and properties of biodegradable poly(butylene succinate)/starch blends. *J. Appl. Polym. Sci.* **2005**, *97*, 257–264.

(26) Fan, D.; Chang, P. R.; Lin, N.; Yu, J.; Huang, J. Structure and properties of alkaline lignin-filled poly(butylene succinate) plastics. *Iran. Polym. J.* **2011**, *20*, 3–14.

(27) Zhao, Y.; Qiu, J.; Feng, H.; Zhang, M. The interfacial modification of rice straw fiber reinforced poly (butylene succinate) composites: Effect of aminosilane with different alkoxy groups. *J. Appl. Polym. Sci.* **2012**, *125*, 3211–3220.

(28) Takasu, A.; Oishi, Y.; Iio, Y.; Inai, Y.; Hirabayashi, T. Synthesis of aliphatic polyesters by direct polyesterification of dicarboxylic acids with diols under mild conditions catalyzed by reusable rare-earth triflate. Structural effects upon enzymatic hydrolysis of poly(butylene succinate-co-ethylene succinate)s. *Macromolecules* **2003**, *36*, 1772–1774.

(29) Mochizuki, M.; Mukai, K.; Yamada, K.; Ichise, N.; Murase, S.; Iwaya, Y. Structural effects upon enzymatic hydrolysis of poly(butylene succinate-co-ethylene succinate)s. *Macromolecules* **1997**, *30*, 7403–7407.

(30) Honda, N.; Taniguchi, I.; Miyamoto, M.; Kimura, Y. Reaction mechanism of enzymatic degradation of poly(butylene succinate-co-terephthalate) (PBST) with a lipase originated from pseudomonas cepacia. *Macromol. Biosci.* **2003**, *3*, 189–197.

(31) Luo, S.; Li, F.; Yu, J.; Cao, A. Synthesis of poly(butylene succinate-co-butylene terephthalate) (PBST) copolyesters with high molecular weights via direct esterification and polycondensation. *J. Appl. Polym. Sci.* **2010**, *115*, 2203–2211.

(32) Luo, F. L.; Luo, F. H.; Xing, Q.; Zhang, X. Q.; Jiao, H. Q.; Yao, M.; Wang, D.; et al. Hydrogen-bonding induced change of crystallization behavior of poly(butylene succinate) in its mixtures with bisphenol A. *Chin. J. Polym. Sci.* **2013**, *31*, 1685–1696.

(33) Dong, T.; He, Y.; Shin, K. M.; Inoue, Y. Formation and characterization of inclusion complexes of poly(butylene succinate) with α-and γ-cyclodextrins. *Macromol. Biosci.* **2004**, *4*, 1084–1091.

(34) Han, S. I.; Lim, J. S.; Kim, D. K.; Kim, M. N.; Im, S. S. In situ polymerized poly(butylene succinate)/silica nanocomposites: physical properties and biodegradation. *Polym. Degrad. Stab.* **2008**, *93*, 889–895.

(35) Jin, H. J.; Kim, D. S.; Kim, M. N.; Lee, I. M.; Lee, H. S.; Yoon, J. S. Synthesis and properties of poly(butylene succinate) with N-hexenyl side branches. *J. Appl. Polym. Sci.* **2001**, *81*, 2219–2226.

(36) Lee, S. I.; Yu, S. C.; Lee, Y. S. Degradable polyurethanes containing poly(butylene succinate) and poly(ethylene glycol). *Polym. Degrad. Stab.* **2001**, *72*, 81–87.

DOI: 10.1021/acs.jpcb.7b07954
J. Phys. Chem. B 2017, 121, 9476–9485

(37) Li, Y. D.; Zeng, J. B.; Wang, X. L.; Yang, K. K.; Wang, Y. Z. Structure and properties of soy protein/poly(butylene succinate) blends with improved compatibility. *Biomacromolecules* **2008**, *9*, 3157−3164.
(38) Lin, N.; Yu, J.; Chang, P. R.; Li, J.; Huang, J. Poly (butylene succinate)-based biocomposites filled with polysaccharide nanocrystals: Structure and properties. *Polym. Compos.* **2011**, *32*, 472−482.
(39) Qi, Z. G.; Ye, H. M.; Xu, J.; Chen, J.; Guo, B. H. Improved the thermal and mechanical properties of poly(butylene succinate-co-butylene adipate) by forming nanocomposites with attapulgite. *Colloids Surf., A* **2013**, *421*, 109−117.
(40) Qi, Z. G.; Ye, H. M.; Xu, J.; Guo, B. H.; et al. Synthesis and characterizations of attapulgite reinforced branched poly(butylene succinate) nanocomposites. *Colloids Surf., A* **2013**, *436*, 26−33.
(41) Ojijo, V.; Sinha Ray, S.; Sadiku, R. Role of specific interfacial area in controlling properties of immiscible blends of biodegradable polylactide and poly[(butylene succinate)-co-adipate]. *ACS Appl. Mater. Interfaces* **2012**, *4*, 6690−6701.
(42) Jin, T. X.; Zhou, M.; Hu, S. D.; Chen, F.; Fu, Q.; Fu, Y. Effect of molecular weight on the properties of poly(butylene succinate). *Chin. J. Polym. Sci.* **2014**, *32*, 953−960.
(43) Lim, J. S.; Hong, S. M.; Kim, D. K.; Im, S. S. Effect of isocyanate-modified fumed silica on the properties of poly(butylene succinate) nanocomposites. *J. Appl. Polym. Sci.* **2008**, *107*, 3598−3608.
(44) Phua, Y. J.; Chow, W. S.; Mohd Ishak, Z. A. The hydrolytic effect of moisture and hygrothermal aging on poly(butylene succinate)/organo-montmorillonite nanocomposites. *Polym. Degrad. Stab.* **2011**, *96*, 1194−1203.
(45) Phua, Y. J.; Lau, N. S.; Sudesh, K.; Chow, W. S.; Mohd Ishak, Z. Biodegradability studies of poly(butylene succinate)/organo-montmorillonite nanocomposites under controlled compost soil conditions: effects of clay loading and compatibilizer. *Polym. Degrad. Stab.* **2012**, *97*, 1345−1354.
(46) Hexig, B.; Alata, H.; Asakawa, N.; Inoue, Y. Novel biodegradable poly(butylene succinate)/poly(ethylene oxide) blend film with compositional and spherulite-size gradients. *J. Polym. Sci., Part B: Polym. Phys.* **2005**, *43*, 368−377.
(47) Ye, H. M.; Wang, R. D.; Liu, J.; Xu, J.; Guo, B. H. Isomorphism in poly(butylene succinate-co-butylene fumarate) and its application as polymeric nucleating agent for poly (butylene succinate). *Macromolecules* **2012**, *45*, 5667−5675.
(48) Khasanah; Reddy, K. R.; Ogawa, S.; Sato, H.; Takahashi, I.; Ozaki, Y. Evolution of intermediate and highly ordered crystalline states under spatial confinement in poly(3-hydroxybutyrate) ultrathin films. *Macromolecules* **2016**, *49*, 4202−4210.
(49) Charlon, S.; Delbreilh, L.; Dargent, E.; Follain, N.; Soulestin, J.; Marais, S. Influence of crystallinity on the dielectric relaxations of poly(butylene succinate) and poly [(butylene succinate)-co-(butylene adipate)]. *Eur. Polym. J.* **2016**, *84*, 366−376.
(50) Di Lorenzo, M. L.; Androsch, R.; Righetti, M. C. Low-temperature crystallization of poly(butylene succinate). *Eur. Polym. J.* **2017**, *94*, 384−391.
(51) Ye, H. M.; Chen, X. T.; Liu, P.; Wu, S. Y.; Jiang, Z.; Xiong, B.; Xu, J. Preparation of poly(butylene succinate) crystals with exceptionally high melting point and crystallinity from its inclusion complex. *Macromolecules* **2017**, *50*, 5425−5433.
(52) Noda, I. Two-dimensional infrared spectroscopy. *J. Am. Chem. Soc.* **1989**, *111*, 8116−8118.
(53) Ozaki, Y.; Liu, Y.; Noda, I. Two-dimensional near-infrared correlation spectroscopy study of premelting behavior of nylon 12. *Macromolecules* **1997**, *30*, 2391−2399.
(54) Li, W.; Sun, B.; Wu, P. Study on hydrogen bonds of carboxymethyl cellulose sodium film with two-dimensional correlation infrared spectroscopy. *Carbohydr. Polym.* **2009**, *78*, 454−461.
(55) Van Krevelen, D. W. Properties of polymers: their correlation with chemical structure; their numerical estimation and prediction from additive group contributions. *Properties of Polymers*, 3rd ed.; Elsevier: 1990; pp 109−127.
(56) Fakhraai, Z.; Forrest, J. A. Measuring the surface dynamics of glassy polymers. *Science* **2008**, *319*, 600−604.
(57) Kerle, T.; Lin, Z.; Kim, H. C.; Russell, T. P. Mobility of polymer at the air/polymer interface. *Macromolecules* **2001**, *34*, 3484−3492.
(58) Wallace, W. E.; Fischer, D. A.; Efimenko, K.; Wu, W. L.; Genzer, J. Polymer chain relaxation: surface outpaces bulk. *Macromolecules* **2001**, *34*, 5081−5082.
(59) Paeng, K.; Swallen, S. F.; Ediger, M. D. Direct Measurement of molecular motion in freestanding polystyrene thin film. *J. Am. Chem. Soc.* **2011**, *133*, 8444−8447.

DOI: 10.1021/acs.jpcb.7b07954
J. Phys. Chem. B 2017, 121, 9476−9485